ACS OMEGA

Open Access



http://pubs.acs.org/journal/acsodf

Article

# Experimental Study of the Effect of CO/$H_2$ Ratio and Release Pressure on Syngas Jet Flame Propagation and Overpressure

Zheng Li, Langqing Lu, Min Yao,* Zhilei Wang, Zhenmin Luo, Qianrui Huang, Tongshuang Liu, and Xuhai Pan*

Cite This: *ACS Omega* 2024, 9, 36961−36968

Read Online

ACCESS | Metrics & More | Article Recommendations

**ABSTRACT:** Syngas, composed of hydrogen and carbon monoxide, serves as an alternative fuel for hydrogen energy and a key raw material for chemical synthesis. However, due to its flammable nature, syngas poses risks of forming explosive mixtures in the event of a leak. This study explores potential accident scenarios in coal chemical environments involving syngas reaction vessels. Experimental investigations focus on the overpressure and propagation dynamics of jet flames resulting from syngas leakage, with CO volume fractions ranging from 50 to 80% and release pressures between 2 and 5 MPa. Results reveal that maximum flame overpressure occurs within a CO volume fraction range of 55−65%, with no consistent relationship observed between overpressure and CO fraction at fixed release pressures. During our experiments, the maximum recorded overpressure of 28.4 kPa was reached during vented explosions. Additionally, ignition outcomes categorize into three types based on flame propagation speed: combustion/flare, resembling normal deflagration; and high-velocity deflagration, characterized by rapid propagation and potential for steady jet fire formation. While shockwave-like features may be observed, these do not indicate true detonation. These findings offer insights for the safe handling and storage of syngas.

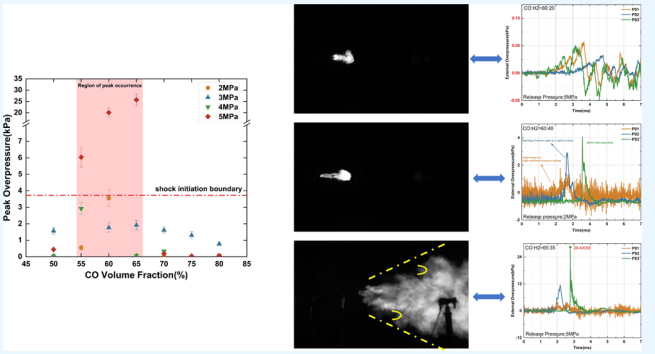


## 1. INTRODUCTION

Hydrogen energy has been widely explored as a possible solution to the energy and ecological crises. Syngas, a mixture of carbon monoxide and hydrogen, has significant potential as a low-carbon, high-efficiency, renewable and clean fuel.[1] Industrial syngas, with harmful components such as $H_2S$, $SO_x$, and heavy metals removed, is commonly used in gas boilers, gas turbines, and other gas appliances,[2] or as a raw material for chemical synthesis. Syngas can be prepared from various sources, such as coal gasification,[3−5] gasification of biomass waste,[6,7] and refinery residues.[8,9] Currently, coal gasification is the primary source of syngas.[10] Syngas has more complex combustion and explosion characteristics compared to traditional hydrocarbon fuels. The combustion and explosion characteristics of syngas need to be studied with a focus on the proportion of its fuel components. The significant physicochemical differences between hydrogen and carbon monoxide, the two primary components of syngas, result in varying combustion behaviors. Additionally, the ratio of these components can change widely depending on the gasification process employed, influencing the combustion characteristics of the syngas mixture.

Investigating the safety of accidental releases is crucial for the safe use of syngas as a fuel and chemical feedstock. Syngas stored under pressure can lead to accidental leakage due to overpressure in storage tanks or vessel breakage, which can result in the generation of jet flames.[11] The generation of a jet fire can produce shock overpressure and heat radiation that can affect personnel and equipment downstream, potentially leading to a domino effect and causing a larger accident. Guo et al.[12] investigated the propagation characteristics of high-pressure hydrogen jet flames for pure hydrogen jet flame studies. Additionally, Pitts et al.[13] demonstrated the significant impact of fuel concentration on jet fire hazard. Wang and Sun[14] summarized the minimum ignition energy and explosion limit study for syngas components in the study of syngas combustion and explosion characteristics. The impact of temperature, pressure, humidity, and the degree of turbulence was also considered. In a study by Sun,[15] the explosion characteristics of syngas with different component ratios were investigated in a

Received: January 11, 2024
Revised: August 2, 2024
Accepted: August 16, 2024
Published: August 21, 2024

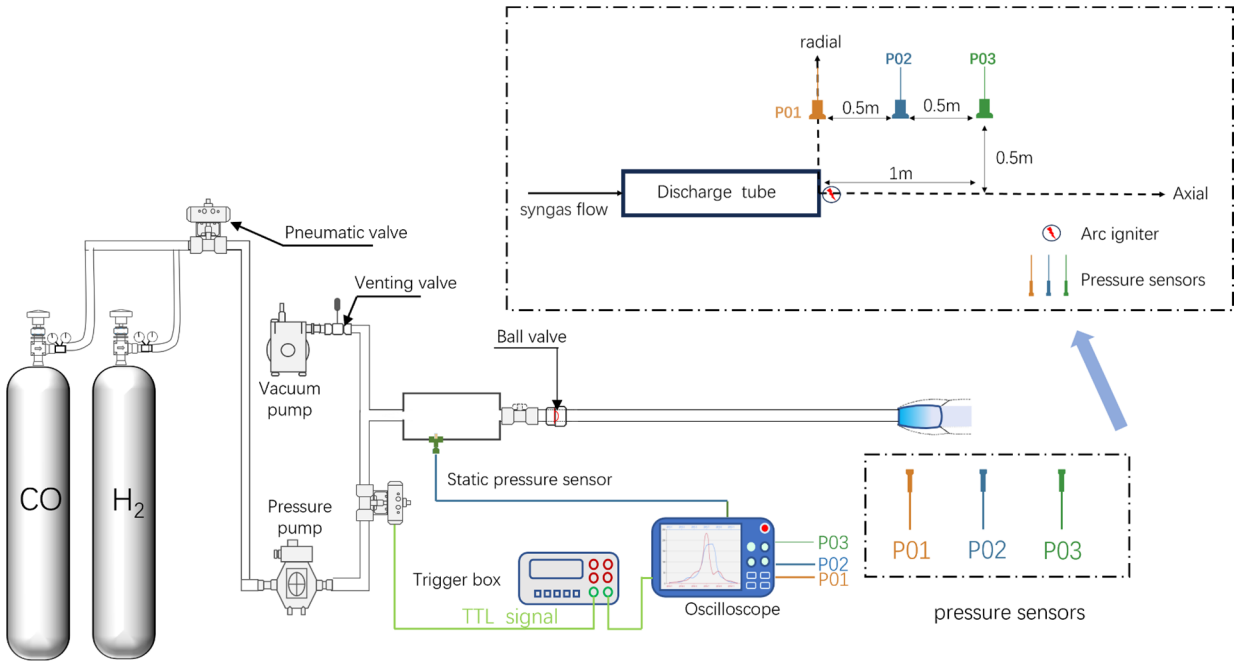


**Figure 1.** Schematic diagram of the experimental system.

constant volume explosion sphere. The results showed that an increase in the proportion of hydrogen led to an increase in the maximum explosion pressure. Sun's[16] turbulent explosion experiments presented similar conclusions, showing that a higher proportion of hydrogen resulted in a higher explosion overpressure due to its greater combustion range, diffusivity, laminar flame speed, and explosion index.[17]

The conventional method for investigating jet flame hazards involves igniting the jet at the orifice using forced ignition.[18] Shy et al.[19−21] investigated the effect of different component ratios, initial pressures, and turbulence degrees on the propagation velocity of outwardly propagating syngas flames. To evaluate the hazard of jet flames, Zhang et al.[22] investigated the thermal radiation hazard of propane jet fires, while Guo et al.[12] studied the overpressure hazard of forced ignition of hydrogen jets. It is worth noting that the ignition position has a significant effect on the overpressure. Several studies have attempted to mitigate the overpressure hazard of jet flames by using walls.[23,24]

Previous studies have primarily focused on the NOx emission characteristics of syngas as a fuel in nonpremixed jet flames used in burners.[25,26] However, there has been limited research on the hazard assessment of syngas jet flames, particularly in relation to overpressure hazards. This paper employs an experimental study to investigate the overpressure hazard downstream of a syngas jet being forced to ignite for a coal gasification-to-syngas scenario with CO volume ratios ranging from 50 to 80% and release pressures of 2−5 MPa, encompassing the operational conditions of most coal gasification reactors. The purpose of this paper is to provide guidance on the placement and configuration of syngas reactors and high-pressure storage vessels, as well as to examine the impact of the hydrogen/carbon monoxide volume ratio and release pressure on the overpressure of syngas jet flames.

## 2. RESEARCH METHODOLOGY

**2.1. Experimental Setup.** This paper describes the experimental platform shown in Figure 1, which consists of four parts: a gas supply system, a high-pressure storage tank, a pipeline evacuation and ignition system, and a data acquisition system. The gas supply system comprised one 40 L bottle of 99.999% pure hydrogen, one 40 L bottle of 99.999% pure carbon monoxide, and one 99.99% pure nitrogen bottle for purging after each experiment. The tank has a volume of 4 L and is equipped with a vacuum pump, an emergency venting valve, and an inbuilt pressure transducer (Kulite, 375M-250BARSG) for real-time pressure monitoring. The evacuation and ignition system comprises a pneumatic ball valve and a seamless steel pipe, 1.7 m in length and 10 mm in diameter, and the experiment uses an arc igniter to generate a stable arc for forced ignition. The pneumatic ball valve's fully open time was set to 100 ms to prevent spontaneous combustion of the syngas in the pipeline due to shock waves.[27] The data acquisition system utilizes three PCB-106B ICP acoustic pressure sensor (measurement Range: 57.2 kPa, resolution: 0.00069 kPa), labeled P01, P02, and P03, to record the pressure history outside the drain tube. The sensor locations are arranged as shown in the dashed box in Figure 1. Data was acquired and recorded using an oscilloscope (HIOKI, MR6000) with a sampling rate of 20 M/s and a total sampling time of 5s for each pass. The jet and flame propagation process in the near-field of the tube orifice was filmed using a high-speed camera (Phanton, V2512) set to a frame rate of 10,000 fps, a resolution of 1024 × 640, and an exposure duration of 70 $\mu$s. The pressure data outside the pipe is obtained using three pressure sensors, namely P01, P02, and P03, which are connected to the oscilloscope. The trigger line of the high-speed camera is also connected to the oscilloscope. Both the oscilloscope and the high-speed camera start working when the pressure sensors in the tank detect a pressure drop. The text includes colorful flame pictures captured using regular cameras. The electric arc igniter is used as the ignition device and is placed at 0.05, 0.5, and 1.0 m downstream of the pipe mouth axis. The arc is generated at the same height as the nozzle and the igniter is securely fixed to the ground to prevent any displacement caused by the airflow during discharge.

**2.2. Experimental Procedures.** The paper investigates the impact of the volume ratio of hydrogen/CO in syngas and the


https://doi.org/10.1021/acsomega.4c00357
ACS Omega 2024, 9, 36961−36968

release pressure on the experimental variables. Two sets of ignition position change conditions are used to introduce typical pressure waveforms. At the start of the experiment, the pressure of the gas supply system's cylinder pressure-reducing valve was adjusted to allow the two gases to enter the storage tank sequentially and reach the specified relief pressure in the tank. As the release pressure ranges between 2 and 5 MPa, it is recommended to use the gas compression factor equation to determine the pressure outlet setting of the pressure reducing valve. This will ensure that the gas volume ratio in the tank is correct, as demonstrated in eq 1.

$$PV = ZnRT \quad (1)$$

Pressure $(P)$ is measured in pascals (Pa), while temperature $(T)$ is measured in Kelvin (K). The compression factor, $Z$, is a dimensionless parameter that represents the deviation of the actual gas from the ideal gas law at a given temperature and pressure.

Before the experiment, the storage tank was vacuumed using a vacuum pump. Then, the tank was filled with two gases. After the gas filling was completed, the tank was left to stand for a period of time to allow the gases to mix completely. Next, the arc igniter was switched on, and a pneumatic ball valve was remotely opened using a remote control device. The syngas jet was released into the atmosphere through a bleeder tube and could be ignited on contact with the arc igniter. Finally, each release was followed by a nitrogen purge to remove any residual syngas from the release tube.

## 3. RESULTS AND DISCUSSION

**3.1. Typical Experimental Conditions.** Figure 2 shows the relief pressure history recorded by the P03 sensor. The discharge

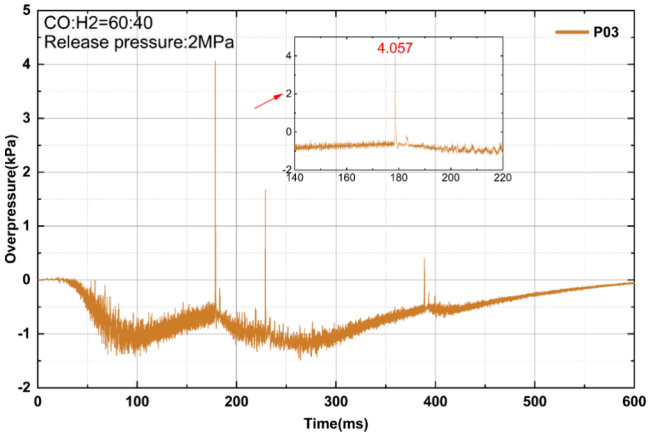


**Figure 2.** Full pressure recording of a typical discharge.

pressure was 2 MPa, the volume ratio of the released syngas was 60% hydrogen to 40% carbon monoxide, and the ignition position was 0.05 m from the tube outlet, under which condition the syngas jet was successfully ignited. To better demonstrate the full pressure change process, we manually selected the zero time point. This point does not indicate the absolute time of arrival of the pressure wave". When the sensor receives an initial pressure fluctuation, the magnitude of the pressure fluctuation is low, only a small amount of gas is vented in the predischarge phase and ignition has not yet occurred. As the release continues, the discharge of syngas increases along with the gas flow rate. The sensor detects a negative pressure phase, which lasts approximately 600 ms. After the pneumatic ball valve is closed, the upstream pressure decreases, and the discharge gradually ceases. However, the figure shows three distinct pressure peaks resulting from a sudden increase in pressure, indicating that the syngas jet was ignited multiple times. The maximum pressure peak, shown in the locally enlarged area in Figure 2, reached a maximum overpressure of 4.057 kPa. In other tests, the syngas jet was ignited several times, as often happens. The highest value of overpressure during the entire release process is noted as the peak pressure.

Figure 3 illustrates the influence of ignition position on the ignition characteristics of syngas gas jet flames. Figure 3a,b depicts the flame propagation process images when ignited at positions 0.05 and 0.5 m along the axis at the nozzle outlet, respectively, to compare the effect of ignition position on synthetic gas jet flames. The appearance of the visible flame in the preceding frame is defined as time zero.

In Figure 3a, for ignition at the position of 0.05 m from the nozzle outlet, the initial phase of the jet flame appears blue. As the flame propagates downstream, its combustion intensifies, accompanied by an increase in brightness at the leading edge. At around 40 ms, the combustion reaches its peak intensity, characterized by a white glare. Additionally, the flame lift-off height gradually increases. However, the flame exhibits some instability, with intermittent occurrences at 210 ms, followed by the formation of a relatively stable self-sustained flame around 370 ms. The color of the flame transitions from blue in the early stages to orange-red later on. During transient jet release, better mixing between the jet front and the surrounding air occurs, whereas steady-state jet flames lack this condition. Consequently, the brightness of the steady jet flame is lower compared to that at 40 ms.

In contrast, ignition at the 0.5 m position (Figure 3b) results in significantly reduced flame combustion intensity, evident from the diminished flame area and brightness. The flame appears pale blue and has a shorter duration. Partial ignition of the surrounding and downstream synthetic gas jet by the igniter leads to an intermittent flame pattern. Furthermore, sensor data indicate no pressure fluctuations exceeding the airflow noise level for ignition at the 0.5 m axial position, suggesting negligible pressure damage downstream. This can be attributed to the lower jet velocity downstream, reducing the efficiency of gas-air mixing, and resulting in a lower gas concentration differential. Therefore, all subsequent tests in this study utilize ignition at the 0.05 m axial position to determine the maximum overpressure that synthetic gas jet flames may generate.

**3.2. Syngas Ignition Results.** When a high-pressure syngas is released through a pipeline and encounters an igniter, the results can be classified into four categories: combustion/flash flame at lower overpressure, normal deflagration, high velocity deflagration at higher pressures, and nonignition. The three scenarios other than nonignition are described below.

Figure 4 displays the occurrence of low overpressure combustion. The CO volume fraction is 80% and the release pressure is 5 MPa. The occurrence of low overpressure combustion or flash combustion is characterized by a lower peak overpressure, with the highest overpressure in the figure being only 0.057 kPa. Furthermore, the process of increasing overpressure is slow and lacks strong discontinuity, indicating that the pressure perturbation has not yet formed a shock wave. The flames are also subsonic, suggesting low downstream overpressure and flame hazard in this scenario.


https://doi.org/10.1021/acsomega.4c00357
ACS Omega 2024, 9, 36961−36968

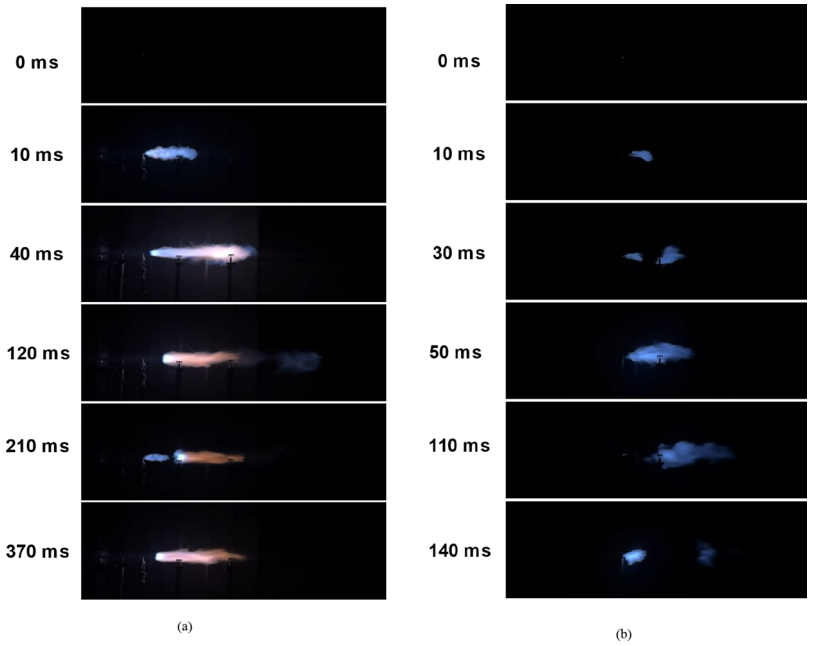


**Figure 3.** Flame propagation at different ignition firing positions at 3 MPa. (a) Ignition at 0.05 m; (b) Ignition at 0.5 m.

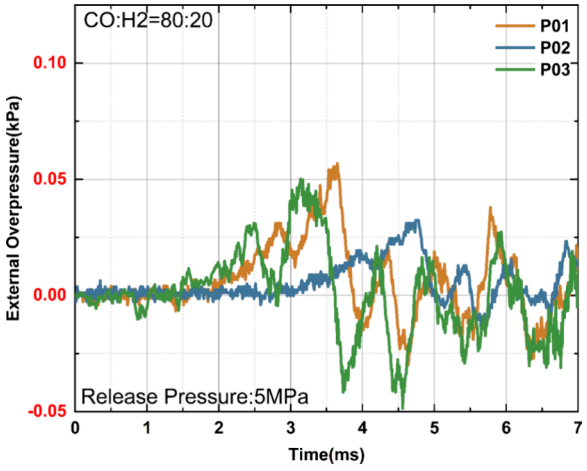


**Figure 4.** Pressure profile of combustion/flash flame.

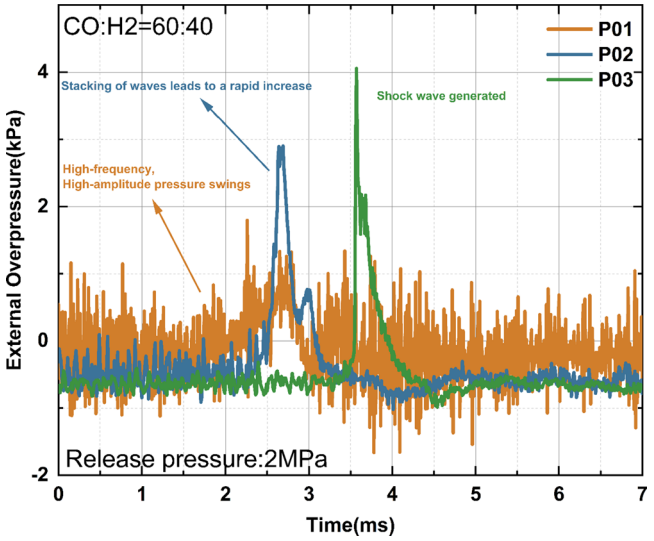


**Figure 5.** Pressure profile of normal deflagration.

Figure 5 illustrates the scenario of a 2 MPa release pressure with a CO proportion of 60%. Under these conditions, the syngas jet flame undergoes a typical deflagration, characterized by features resembling shockwaves in the pressure history recorded by sensor P03, though these do not indicate a true detonation. The pressure fluctuation processes of sensors P01, P02, and P03 reveal the formation of the leading shockwave during the ignition of the synthetic gas jet flame. The P01 curve exhibits minor pressure fluctuations accompanied by small increments, indicating relatively large disturbances. The P02 curve depicts the gradual stacking of pressure waves, with an accelerated rate of pressure rise, yet without any pressure discontinuity at this stage. Upon reaching sensor P03, the pressure wave has formed into a strong discontinuity, namely, the shockwave. The significant pressure gradient ahead and behind the shockwave causes a sharp increase in pressure recorded by sensor P03. The gradual formation of the shockwave suggests that ignition outside the synthetic gas jet pipe differs from the deflagration process inside a combustible gas container. The formation of the shockwave requires time and flame development distance. However, due to the limited number of sensors, it is not possible to calculate the exact speed of the shockwave, and consequently, it is uncertain whether this phenomenon constitutes detonation of the synthetic gas outside the pipe. Therefore, we conservatively consider this combustion phenomenon to be deflagration, where the flame propagation speed exceeds the speed of sound. The combustion phenomenon in the high-speed jet is different from the premixed gas in the pipe deflagration in the detonation of the bombardment. Additionally, more pressure sensors are required to determine whether the intensity of the shock wave increases following the P03 sensor.

In the case of the high velocity deflagration with very high overpressure shown in Figure 6, the peak overpressure is a prominent feature, reaching up to 28.40 kPa, which is significantly higher than the previous case. The pressure trends of the three sensors resemble those of a typical deflagration.



https://doi.org/10.1021/acsomega.4c00357
ACS Omega 2024, 9, 36961−36968

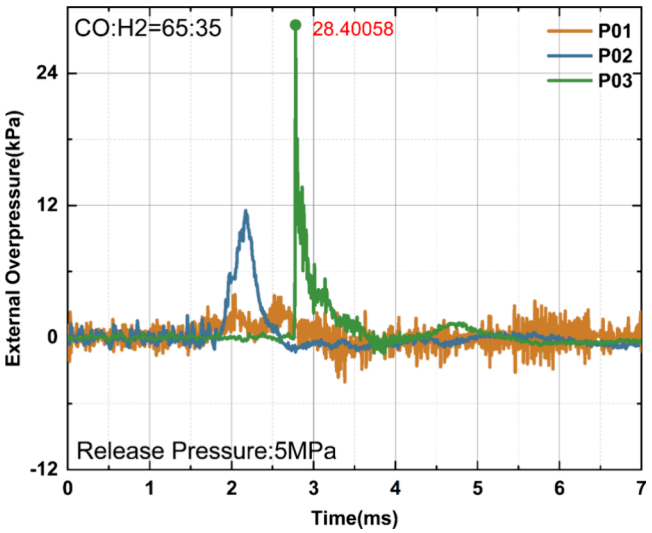


**Figure 6.** Pressure profile of high velocity deflagration.

However, there is a significant difference in the peak and rate of pressure rise between P01 and P02, indicating a rapid pressure shift in the area between the two sensors. It should be noted that the peak overpressure of P03 may not accurately represent the hazards of the high overpressure deflagration due to the placement of the pressure sensor and the potential continuation of the pressure wave superposition after the P03 sensor. To ensure a more accurate assessment of the hazards, the pressure sensor should be placed axially to the orifice and the superposition of the pressure wave should be taken into consideration. The literature summarizes the hazardous pattern of explosion overpressure on people and buildings.[28,29] In our experiments, the maximum recorded overpressure reached 28.4 kPa, which is sufficient to cause damage such as the deformation of metal panels and minor damage to concrete walls. This very high overpressure case differs significantly from the first two ignition cases in terms of flame propagation, which will be discussed in detail in Section 3.4.

**3.3. Effect of Release Pressure and Carbon Monoxide Fraction of Syngas on Maximum Overpressure.** Figure 7 shows the effect of the volume fraction of carbon monoxide in the syngas on the peak flame overpressure at different release pressures. The nonignition test cases are not plotted in the figure. The figure illustrates that there is no consistent pattern for the volume fraction of CO in the syngas for flame overpressure at a specific release pressure. Additionally, the nonignition conditions occur at release pressures of 2, 3, and 4 MPa. However, the maximum overpressure occurs within the range of 55−65% CO fraction at each release pressure. This suggests that hydrogen/carbon monoxide mixtures in the group distribution are more hazardous than those within that range. In Figure 7, the dotted line represents the boundary between the pressure record with and without shock generation. For the experimental conditions described in this paper, the boundary is at approximately 3.27 kPa at 4 MPa with 55% of the released CO fraction and 4.06 kPa at 2 MPa with 60% of the released CO fraction. The present experiments indicate that the deflagration of syngas outside of the tube did not generate a shock wave in most conditions, and the combustion was subsonic. However, in four conditions, a shock wave was produced. Furthermore, a higher fraction of carbon monoxide results in lower flame overpressure, as shown by Table 1, which presents some physical

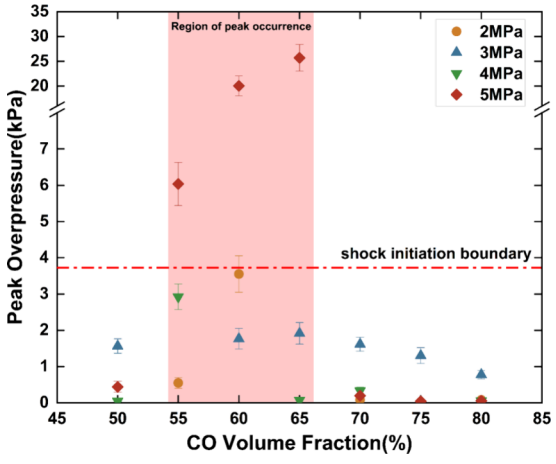


**Figure 7.** Volume fraction of carbon monoxide in syngas for peak flame overpressure plots at different release pressures.

**Table 1. Details of Measurement and Data Collection Instruments**

| gas type | $H_2$ | CO |
|---|---|---|
| flammability limit (%) | 4−75 | 12.5−74.2 |
| standard heat of combustion (kJ/mol) | 285.8 | 283.3 |
| diffusion Coefficient at atmospheric pressure and room temperature ($cm^2/s$) | 0.61 | 0.16 |

parameters of the two gases. When a homogeneous mixture of the gases is ejected from the tube, the heat of combustion is less influenced by its components, while the flammability limit and gas diffusion coefficient play a more significant role.

The low diffusion coefficient of carbon monoxide results in less efficient mixing of the high carbon monoxide syngas as the oxidant undergoes a limited mixing process. Another piece of information shown in Figure 7 is that the three conditions with the highest overpressure occur at a release pressure of 5 MPa, indicating that the jet velocity of the syngas at the nozzle has a significant effect on the flame overpressure. The higher the jet velocity at the orifice, the more the syngas-air shear layer at the jet boundary sucks in air, and the more intense the turbulent combustion flame. However, under these experimental conditions, the hydrogen/CO jet at the orifice is in an underexpanded state.[30] As a result, the high release pressure leads to higher jet pressure behind the Mach disc, which promotes more intense combustion chemistry. Furthermore, increasing the release pressure results in a higher mass flow rate from the tube to the outlet of the fixed-volume tank in the experiment. This leads to an increase in concentration downstream of the jet, contributing to the growth of the flame maintenance time and flame length. As a result, there is a boost to the continuous superposition of the combustion pressure wave.

**3.4. Syngas Jet Flame Propagation Characteristics.** A high-speed camera was used to observe the various flame development and propagation processes at a fixed position after igniting the syngas jet under different overpressure conditions. The connection between flame overpressure and the observed differences in flame propagation processes was elucidated.

Figure 8 shows a group plot of the key frames of the flame propagation process for the test condition (same condition as in Figure 4) with a CO volume fraction of 80% and a release


https://doi.org/10.1021/acsomega.4c00357
ACS Omega 2024, 9, 36961−36968

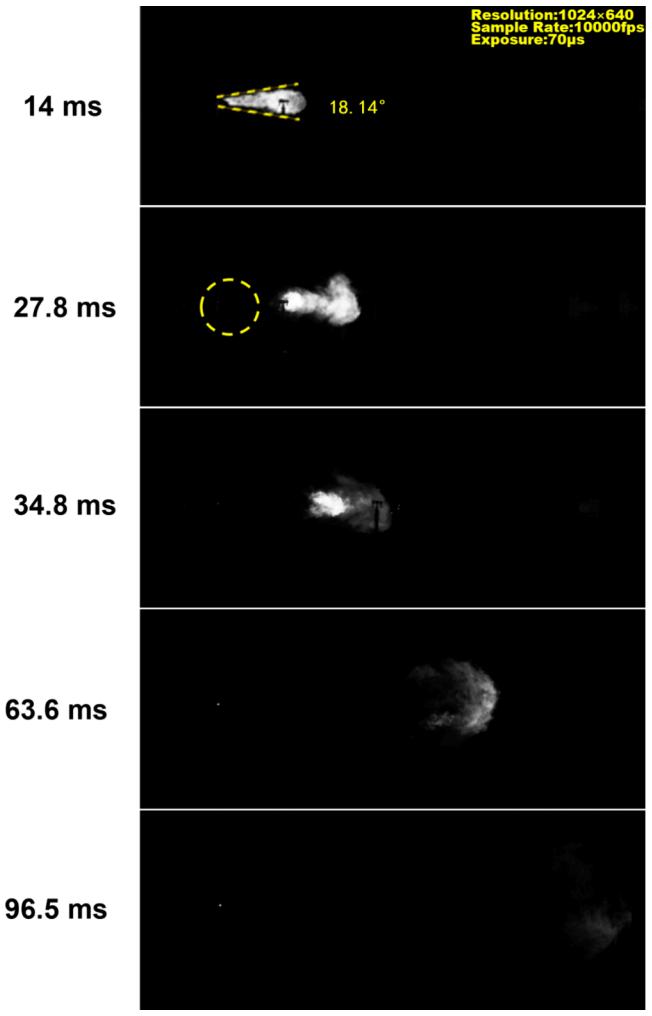


**Figure 8.** Low overpressure deflagration flame propagation diagram.

pressure of 5 MPa, with a brightness change at the orifice appearing as time zero. The figure shows that the flame duration phase, from ignition to the disappearance of the visible flame on the screen, lasts approximately 97 ms. The jet flame initially takes on a conical shape to propagate downstream and then grows in flame propagation. At 14 ms, the angle presented by the jet flame is 18.14°, which is smaller than the "normal deflagration" scenario mentioned later in the text. However, at 27.8 ms, asymmetric flame propagation along the axial direction is observed. Concurrently, flame extinction near the ignition point occurs, with the flame base shifting downstream, ultimately resulting in an inability to sustain the flame and causing an overall reduction in flame length. The near-field flame close to the tube exhibits asymmetry, which suggests a high level of flame propagation instability at this stage. This is due to momentum dominance rather than buoyancy dominance. The reasons for this phenomenon are mainly as follows: First, the expansion effect of the airflow at the orifice is an important influencing factor. The under-expanded jet ejected from the orifice expands and cools down, which reduces the degree of combustion. Second, as the flame gradually propagates downstream, vortex structures develop and affect the upper part of the flame by 27.8 ms. The absence of combustion at the base of the flame (indicated by the yellow dashed circle in Figure 8) leads to an inability to sustain the combustion, resulting in a weakening of the flame. At 34.8 ms, a decrease in brightness at the leading edge of the flame is observed, indicating a reduction in combustion intensity. The flame size significantly shrinks, with no signs of expansion toward the outer periphery of the jet. The flame disappears gradually at 96.5 ms. The pressure fluctuations in this case are solely generated by the initial jet flame. As the combustion is not intense, the resulting combustion pressure wave is already weak by the time it reaches the sensor.

Figure 9 illustrates the flame propagation corresponding to the pressure history presented in Figure 5, with a CO ratio of

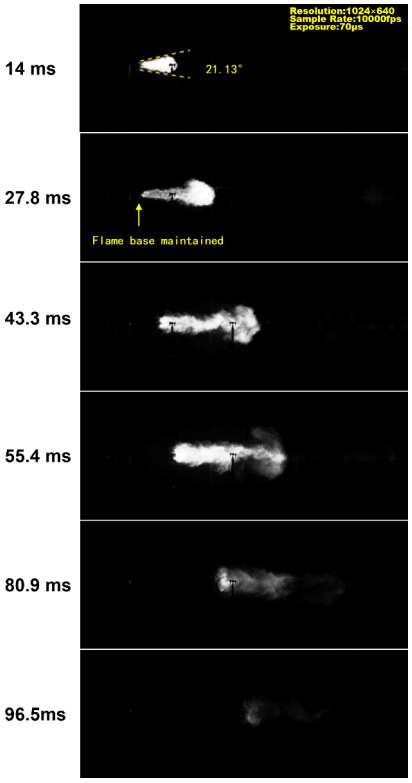


**Figure 9.** Normal deflagration flame propagation diagram.

60% and a release pressure of 2 MPa. In this case, the maximum peak overpressure exceeds 4 kPa, but the flame propagation process is generally similar to that of the previous deflagration type with low overpressure. The flame persistence process also lasts approximately 97 ms. The discrepancy lies in the heightened luminosity and increased combustion observed in the deflagration flame at both 14 and 27.8 ms. Furthermore, there is a degree of sustained combustion at the base of the flame. Specifically, during the early phases of the flame, the deflagration flame demonstrates a broader angle of 21.13°, indicative of its propagation to the outermost periphery of the jet, where the mixing of syngas and air is most efficient. Additionally, there is a more robust maintenance of combustion at the flame's base, intensifying the downstream combustion kinetics. Within the jet, vigorous combustion reactions occur, culminating in the formation of a luminous fireball at the flame's forefront. The fireball exhibits notable gradients in physical parameters, prompting the formation and enlargement of vortices at 43.3 ms. Subsequently, the fireball undergoes displacement from the primary flame body and dissipates by 55.4 ms.

When high overpressure deflagration occurs, as shown in Figure 10 with a CO ratio of 65% and a release pressure of 5 MPa, the most notable feature is the rapid flame propagation


https://doi.org/10.1021/acsomega.4c00357
ACS Omega 2024, 9, 36961−36968

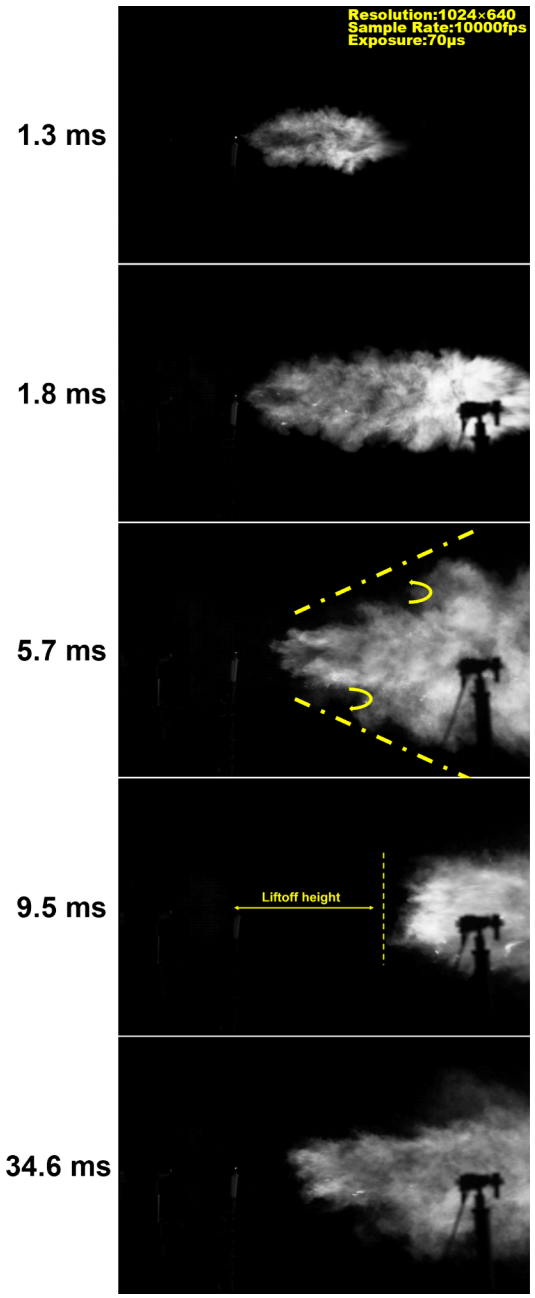


**Figure 10.** High-velocity deflagration flame diagram.

process. In approximately 40 ms, due to an increase in lift-up height, the flame has left the high-speed camera's field of view. At 1.8 ms, the flame has propagated to the far right of the screen. The axial propagation of the flame is slower than its axial propagation at this stage. At 5.7 ms, the flame takes on a conical shape. Intense air entrainment in the shear layer can be observed, causing the lift-up height to increase continuously due to the rise in jet velocity. The flame propagation remains stable, and the base of the flame burns intensely as the lift-up height continues to increase.

In both cases, the flame is not stably maintained, and narrow flame widths are observed during combustion/flash fire at lower overpressure levels and normal deflagration. The concentration of gas inside the jet near the orifice is high, and the combustion of the flame depends on the proper mixing of syngas and air. When the jet is initially ejected from the orifice, a combustible zone is formed by the front of the jet and the air mixed at the edges, which is the condition for the initial combustion of the syngas.

## 4. CONCLUSIONS

This study investigates the phenomena of overpressure and flame propagation induced by syngas flames released at pressures ranging from 2 to 5 MPa and carbon monoxide concentrations between 50% and 80%, following venting through a pipe and ignition by an arc igniter. The investigation is primarily based on pressure data and flame propagation images. The key conclusions drawn from this study are summarized as follows:

1. The influence of carbon monoxide concentration on overpressure at each release pressure does not follow a singular pattern. However, it is observed that the maximum overpressure consistently occurs within the range of 55−65% at all release pressures.
2. Syngas ignition leads to three distinct types of ignition events: combustion/flash fire at lower overpressure levels, normal deflagration, and high-velocity deflagration at higher pressures. Classification is based on the presence or absence of shock wave generation and differences in flame propagation dynamics. High-velocity deflagration events can generate maximum overpressures of up to 28 kPa, posing a potential risk of damage to concrete structures.
3. The combustion/flash fire phenomenon observed at lower overpressure levels is characterized by a failure to form a stable jet of fire. In contrast, high-velocity deflagration events exhibit rapid flame propagation and the formation of a stable jet of fire.

## AUTHOR INFORMATION

### Corresponding Authors

**Min Yao** − *College of Safety Science and Engineering, Xi'an University of Science and Technology, Xi'an 710054, China; Institute of Management Science, Ningxia University, Yin'chuan 750021, China*; Email: ndglym@163.com

**Xuhai Pan** − *College of Safety Science and Engineering, Nanjing Tech University, Nanjing 210009, China*; orcid.org/0000-0002-5309-7817; Email: xuhaipan@njtech.edu.cn

### Authors

**Zheng Li** − *College of Safety Science and Engineering, Xi'an University of Science and Technology, Xi'an 710054, China*; orcid.org/0000-0002-7426-0409

**Langqing Lu** − *College of Safety Science and Engineering, Nanjing Tech University, Nanjing 210009, China*

**Zhilei Wang** − *College of Safety Science and Engineering, Nanjing Tech University, Nanjing 210009, China*

**Zhenmin Luo** − *College of Safety Science and Engineering, Xi'an University of Science and Technology, Xi'an 710054, China*

**Qianrui Huang** − *College of Safety Science and Engineering, Xi'an University of Science and Technology, Xi'an 710054, China*

**Tongshuang Liu** − *College of Safety Science and Engineering, Xi'an University of Science and Technology, Xi'an 710054, China*

Complete contact information is available at: https://pubs.acs.org/10.1021/acsomega.4c00357



https://doi.org/10.1021/acsomega.4c00357
*ACS Omega* 2024, 9, 36961−36968

### Notes

The authors declare no competing financial interest.

## ■ ACKNOWLEDGMENTS

The authors gratefully acknowledge the support by the National Natural Science Foundation of China (No. 52074158), the Ningxia Autonomous Region Key Research and Development Program (No. 2022BEE02001), and the National Key Research and Development Program of intergovernmental international scientific and technological cooperation and innovation special project (No. 2023YFE0199100).

## ■ REFERENCES

(1) Azeem, N.; Beatrice, C.; Vassallo, A.; Pesce, F.; Rossi, R.; Khalid, A. Review and evaluation of metals and alloy's compatibility with hydrogen-fueled internal combustion engines. *Int. J. Engine Res.* **2023**, *24* (9), 4204−4225.

(2) Lieuwen, T. C.; Yang, V.; Yetter, R. A. *Synthesis gas combustion: fundamentals and applications*; CRC Press: Boca Raton, 2010.

(3) Toledo, T. M.; Araus, S. K.; Vasconcelo, A. D. Syngas production from coal in presence of steam using filtration combustion. *Int. J. Hydrogen Energy* **2015**, *40* (19), 6340−6345.

(4) Hong, Y. C.; Lee, S. J.; Shin, D. H.; Kim, Y. J.; Lee, B. J.; Cho, S. Y.; et al. Syngas production from gasification of brown coal in a microwave torch plasma. *Energy* **2012**, *47* (1), 36−40.

(5) Shahbaz, M.; Yusup, S.; Inayat, A.; Patrick, D. O.; Pratama, A.; Ammar, M. Optimization of hydrogen and syngas production from PKS gasification by using coal bottom ash. *Bioresour. Technol.* **2017**, *241*, 284−295.

(6) Shahabuddin, M.; Alam, M. T.; Krishna, B. B.; Bhaskar, T.; Perkins, G. A review on the production of renewable aviation fuels from the gasification of biomass and residual wastes. *Bioresour. Technol.* **2020**, *312*, No. 123596.

(7) Martínez, J. D.; Mahkamov, K.; Andrade, R. V.; Lora, E. E. S. Syngas production in downdraft biomass gasifiers and its application using internal combustion engines. *Renewable Energy* **2012**, *38* (1), 1−9.

(8) Atnaw, S. M.; Sulaiman, S. A.; Yusup, S. Syngas production from downdraft gasification of oil palm fronds. *Energy* **2013**, *61*, 491−501.

(9) Huang, Q. X.; Wang, J.; Qiu, K. Z.; Pan, Z. J.; Wang, S. K.; Chi, Y.; et al. Catalytic pyrolysis of petroleum sludge for production of hydrogen-enriched syngas. *Int. J. Hydrogen Energ* **2015**, *40* (46), 16077−16085.

(10) Fiore, M.; Magi, V.; Viggiano, A. Internal combustion engines powered by syngas: A review. *Appl. Energy* **2020**, *256*, No. 115415.

(11) Gómez-Mares, M.; Zárate, L.; Casal, J. Jet fires and the domino effect. *Fire Safety J.* **2008**, *43* (8), 583−588.

(12) Guo, L.; Ba, Q. X.; Zhang, S. S. Study on hydrogen dynamic leakage and flame propagation at normal-temperature and high-pressure. *Int. J. Hydrogen Energ* **2023**, *48* (70), 27416−27426.

(13) Pitts, W. M.; Yang, J. C.; Prasad, K.; Fernandez, M. Dispersion and Burning Behavior of Hydrogen Released in a Full-Scale Residential Garage in the Presence and Absence of Conventional Automobiles - Supplemental Video Materials. *J. Res. Natl. Inst. Stand. Technol.* **2018**, *123*, 1−3.

(14) Wang, W. Q.; Sun, Z. Y. Experimental studies on explosive limits and minimum ignition energy of syngas: A comparative review. *Int. J. Hydrogen Energ* **2019**, *44* (11), 5640−5649.

(15) Sun, Z. Y. Laminar Explosion Properties of Syngas. *Combust. Sci. Technol.* **2020**, *192* (1), 166−181.

(16) Sun, Z. Y.; Liu, S. Y. A comparative study on the turbulent explosion characteristics of syngas between CO-enriched and H-enriched. *Energy* **2022**, *241*, No. 122941.

(17) Crowl, D. A.; Jo, Y. D. The hazards and risks of hydrogen. *J. Loss Prevent Proc.* **2007**, *20* (2), 158−164.

(18) Schefer, R. W.; Houf, W. G.; Williams, T. C.; Bourne, B.; Colton, J. Characterization of high-pressure, underexpanded hydrogen-jet flames. *Int. J. Hydrogen Energ* **2007**, *32* (12), 2081−2093.

(19) Chiu, C. W.; Dong, Y. C.; Shy, S. S. High-pressure hydrogen/carbon monoxide syngas turbulent burning velocities measured at constant turbulent Reynolds numbers (vol 37, pg 10935, 2012). *Int. J. Hydrogen Energ* **2013**, *38* (11), 4877−4878.

(20) Lin, Y. C.; Jansohn, P.; Boulouchos, K. Turbulent flame speed for hydrogen-rich fuel gases at gas turbine relevant conditions. *Int. J. Hydrogen Energ* **2014**, *39* (35), 20242−20254.

(21) Shy, S. S.; Liu, C. C.; Lin, J. Y.; Chen, L. L.; Lipatnikov, A. N.; Yang, S. I. Correlations of high-pressure lean methane and syngas turbulent burning velocities: Effects of turbulent Reynolds, Damkohler, and Karlovitz numbers. *P Combust Inst* **2015**, *35*, 1509−1516.

(22) Zhang, B.; Liu, Y.; Laboureur, D.; Mannan, M. S. Experimental Study on Propane Jet Fire Hazards: Thermal Radiation. *Ind. Eng. Chem. Res.* **2015**, *54* (37), 9251−9256.

(23) Schefer, R. W.; Merilo, E. G.; Groethe, M. A.; Houf, W. G. Experimental investigation of hydrogen jet fire mitigation by barrier walls. *Int. J. Hydrogen Energ* **2011**, *36* (3), 2530−2537.

(24) Yu, X.; Yan, W. J.; Liu, Y.; Zhou, P. G.; Li, B.; Wang, C. J. The flame mitigation effect of vertical barrier wall in hydrogen refueling stations. *Fuel* **2022**, *315*, No. 123265.

(25) Hwang, J.; Sohn, K.; Bouvet, N.; Yoon, Y. NOx SCALING OF SYNGAS H/CO TURBULENT NON-PREMIXED JET FLAMES. *Combust. Sci. Technol.* **2013**, *185* (12), 1715−1734.

(26) Lee, J.; Park, S.; Kim, Y. Effects of Fuel-Side Nitrogen Dilution on Structure and NO Formation of Turbulent Syngas Non-premixed Jet Flames. *Energ Fuel* **2012**, *26* (6), 3304−3315.

(27) Grune, J.; Sempert, K.; Kuznetsov, M.; Jordan, T. Experimental study of ignited unsteady hydrogen releases from a high pressure reservoir. *Int. J. Hydrogen Energ* **2014**, *39* (11), 6176−6183.

(28) Hu, Q.; Shen, X.; Huang, Z.; Qian, X.; Jiang, J.; Yuan, M.; et al. Shock wave dynamics and venting overpressure hazards induced by indoor premixed hydrogen/air explosion. *Int. J. Hydrogen Energ* **2024**, *51*, 830−847.

(29) Yang, K.; Chen, Y. B.; Xiao, Q. P.; Pang, L. Influence of venting coefficient on disastrous effects of aluminium powder explosions. *Process Saf Environ* **2021**, *156*, 72−88.

(30) Molkov, V.; Saffers, J.-B. Hydrogen jet flames. *Int. J. Hydrogen Energ* **2013**, *38* (19), 8141−8158.



https://doi.org/10.1021/acsomega.4c00357
*ACS Omega* 2024, 9, 36961−36968